RESEARCH ARTICLE

Potentiating microglial efferocytosis by MFG-E8 improves survival and neurological outcome after successful cardiopulmonary resuscitation in mice

Kunxue Zhang[1] | Yuzhen Zhang[1] | Zhentong Li[1] | Jiancong Chen[1] | Yuan Chang[1] | Yongchuan Li[1] | Shuxin Zeng[1] | Sifan Pan[2] | Suyue Pan[1] | Kaibin Huang[1,3]

[1]Department of Neurology, Nanfang Hospital, Southern Medical University, Guangzhou, China

[2]The First Clinical Medical College, Southern Medical University, Guangzhou, China

[3]Department of Neurology, Ganzhou Hospital-Nanfang Hospital, Southern Medical University, Ganzhou, China

Correspondence
Kaibin Huang, Department of Neurology, Nanfang Hospital, Southern Medical University, Guangzhou 510515, China.
Email: hkb@smu.edu.cn

Abstract

Brain injury represents the leading cause of mortality and disability after cardiopulmonary resuscitation (CPR) from cardiac arrest (CA), in which the accumulation of dying cells aggravate tissue injury by releasing proinflammatory intracellular components. Microglia play an essential role in maintaining brain homeostasis via milk fat globule epidermal growth factor 8 (MFG-E8)-opsonized efferocytosis, the engulfment of dying cells and debris. This study investigates whether potentiating microglia efferocytosis by MFG-E8 provides neuroprotection after CA/CPR. After 8-minute asphyxial CA/CPR, male adult C57BL/6J mice were randomly assigned to receive recombinant mouse MFG-E8 (rmMFG-E8) or vehicle. We evaluated the survival and neurological deficits of mice, along with histological damages, phagocytosis index of dying cells, and microglia polarization. A transcriptome analysis was conducted to explore the downstream molecules modulated by MFG-E8. In mice resuscitated from CA, rmMFG-E8 administration significantly enhanced the efferocytosis of apoptotic cells by microglia, improved the survival and neurological function of mice, and attenuated neuropathological injuries. Additionally, rmMFG-E8 induced a prominent alteration in microglial gene expression and promoted a shift from a proinflammatory phenotype to an anti-inflammatory phenotype. Moreover, rmMFG-E8 treatment induced up-regulation of interferon regulatory factor 7 (IRF7), and IRF7 gene silencing largely reversed the neuroprotective effects of rmMFG-E8. This study demonstrates that rmMFG-E8 improves survival and neurological outcomes after CA/CPR by enhancing microglial efferocytosis and reshaping the inflammatory microenvironment in brain tissue. Potentiating MFG-E8 is a promising strategy to combat post-CA brain injury.

KEYWORDS
cardiac arrest, efferocytosis, IRF7, MFG-E8, microglia/macrophage

Kunxue Zhang, Yuzhen Zhang, and Zhentong Li contributed equally to this study.

1 | INTRODUCTION

Sudden cardiac arrest (CA) is a leading contributor to death and morbidity worldwide [1], which occurs to more than 750,000 persons in China annually [2]. Brain injury is the prominent clinical manifestation in patients with successful cardiopulmonary resuscitation (CPR), and its main pathological features include persistent neuroinflammation and neuronal death [3, 4]. The cellular components released by dying cells are part of what drives inflammatory gene expression programs in innate immune cells [5]. Delayed clearance of dying cells further exacerbates tissue injury through cell death-induced inflammation. Microglia serves as brain-resident macrophages, of which a significant function is to maintain brain homeostasis by clearing dying cells and debris through efferocytosis [6, 7]. A growing body of evidence indicates that the efferocytosis of microglia is a fundamental process in facilitating tissue repair and restoration, regulating inflammation, and maintaining the equilibrium of the immune system during homeostasis [8–11]. By contrast, impairment of efferocytosis results in the accumulation of apoptotic cells within inflamed regions, which then proceed to undergo secondary necrosis and cytolysis, releasing intracellular contents that cause tissue damage in the process [8–10, 12].

Milk fat globule epidermal growth factor 8 (MFG-E8) constitutes a fundamental element of milk fat globules from lactating mammary glands [13]. After secretion by activated macrophages, MFG-E8 attaches specifically to apoptotic cells as a bridging molecule, recognizing phosphatidylserine (PS), and targets them to integrin receptors on the phagocytes for engulfment [14, 15]. Increasing studies have demonstrated that MFG-E8 not only plays a crucial role in the phagocytic removal of apoptotic cells but also has therapeutic potential in improving the prognosis of inflammatory diseases [16]. As such, the administration of MFG-E8 for the clearance of apoptotic cells has been demonstrated to suppress the systemic inflammatory response and to confer benefits in sepsis [17].

The protein MFG-E8 is typically expressed on microglia, astrocyte, and vessel endothelial cells in the brain tissue, but mainly on microglia under the pathological state [18]. Previous studies have shown the neuroprotection of supplementation with recombinant MFG-E8 on multiple neurological diseases, including traumatic brain injury, ischemia, and subarachnoid hemorrhage, through inhibiting microglia-involved inflammation and reducing neuronal apoptosis [18–20]. Intriguingly, MFG-E8 treatment drove the conversion of microglia to the anti-inflammatory phenotype, suggesting that MFG-E8 is closely related to the function of microglia besides bridging efferocytosis [20, 21]. Nevertheless, the potential contribution of MFG-E8 within post-CA/CPR brain injury and its mechanisms have not been well studied.

In this study, we evaluated whether exogenous supplementation of MFG-E8 improved neurological outcomes and attenuated histological damage in CA/CPR mice model. In addition, we explored the underlying molecular mechanisms through which MFG-E8 promotes the functional transformation of microglia.

2 | MATERIALS AND METHODS

2.1 | Animals

All experiments were approved by the Animal Care and Use Committee of Nanfang Hospital, Southern Medical University (No. IACUC-LAC-20220708-006) and adhered to the National Institutes of Health Guide for the Care and Use of Laboratory Animals. 8–10 weeks and 20–25 g adult male mice (C57BL/6J) were procured from the Experimental Animal Centre of the Southern Medical University and were reared in a pathogen-free appliances under a 12-h light/dark cycle, with unrestricted access to water and food. Every reasonable attempt was made to limit the number of animals utilized for this investigation and to ensure their well-being.

2.2 | CA/CPR model establishment

The mouse model of asphyxia CA/CPR was established with slight modifications (Figure S1) [22]. Briefly, after anesthetized with isoflurane, mice were connected to a mouse ventilator and cannulated with PE-10 tubes to measure mean arterial blood pressure (MAP) and deliver drugs. Electrocardiograms (ECGs) and rectal temperature were monitored throughout the surgical procedure. The technique of achieving asphyxial CA involved a sudden alteration to the inspiratory gas composition, which was changed to 100% nitrogen. The term "CA" was defined as a MAP decrease below 20 mmHg. Following the cessation of asphyxia, cardiopulmonary resuscitation (CPR) was initiated utilizing mechanical ventilation with the administration of 100% oxygen and epinephrine in a dose of 500 µL (16 µg/mL), along with finger-chest compression at a rate of 300–400 times per minute. Upon achievement of the return of spontaneous circulation (ROSC), chest compression was ceased. Once spontaneous respiratory recovery was achieved, the mice underwent extubation, ventilator weaning, and were subsequently situated in their cages with readily accessible food and water. The detailed process was illustrated in Data S1.

2.3 | Experimental design

A randomization process was used to allocate mice to receive either recombinant mouse MFG-E8 (rmMFG-E8) or a vehicle control 10 min after ROSC. First, the rmMFG-E8 group were given rmMFG-E8 (5 µL, 1 µg/µL in saline, 2805-MF-050, R&D, Minnesota,

USA) via intra-cisterna magna injection (i.c.m.) once [20], whereas the vehicle group were administered with saline in an equivalent volume. The mice that had been successfully resuscitated were then monitored for a period of 7 days to assess their neurological function, as well as their survival rate, their spatial learning and memory capabilities, and any histological injuries that may have occurred. To assess the neuroprotective effects of rmMFG-E8, the remaining mice were evaluated on the 3rd day after CA/CPR. This involved an evaluation of the phagocytosis index and the polarization state of microglia/macrophages. Subsequently, microglia ($CD11b^+/CD45^{med}$) from rmMFG-E8 and vehicle groups on the 3rd day post-CA/CPR were isolated for RNA sequencing to clarify the underlying molecular mechanisms through which MFG-E8 drives microglia to an anti-inflammatory phenotype. A preliminary screen for potential molecules of MFG-E8 that induce microglia to adopt an anti-inflammatory phenotype was conducted using transcriptome analysis, followed by further validation through RNA silencing experiments.

2.4 | Survival rate and neurological outcome evaluation

The number of surviving mice was recorded daily for 7 days following the ROSC. Two investigators, unaware of the animal group assignment, employed a previously reported neurological function scoring system to assess neurological deficits on the 3rd and 7th day in all post-ROSC mice [23]. The scoring system was based on three parameters including screen test, balance beam test, as well as prehensile-traction test. Mice with a total 9 score were regarded as normal.

2.5 | Behavioral analysis

2.5.1 | Open field test

The open field test was conducted on the 3rd day following CA/CPR to assess gross motor function and general mobility in mice. In summary, mice were placed in a $50 \times 50 \times 50$ cm box and permitted to roam freely within it for a period of 10 min. The total distance travelled by the mice was objectively quantified via an automated system for animal behavior analysis (JLBehv-LAM-4, Jiliang Software Technology, Shanghai, China).

2.5.2 | Morris water maze test

In order to evaluate the mice's spatial learning and memory abilities, the Morris water maze test was conducted from the 8th day onwards post-CA/CPR, including experiments on spatial exploration and directional

navigation, as described previously [24]. To investigate the spatial exploration ability in mice, the animals were placed in four different starting points of four quadrants in the pool, with the time the mice spent to locate the hidden platform within 60 s was recorded as the escape latency. The latency was recorded as 60 s if the mice could not locate the target platform within 60 s. The investigator guided mice to the target place and permitted them to remain there for 10 s. This process was repeated 5 days, with the goal of completing the training process.

In terms of directional navigation test, investigator removed the platform permitting mice to explore freely for 60 s. A record was kept of the platform crossings number, as well as the percentage of total time spent in the designated quadrant. All data during the experiment were recorded via an automated system for animal behavior analysis (JLBehv-MWMM, Jiliang Software Technology, Shanghai, China).

2.6 | Laser speckle flowmetry

We conducted laser speckle imaging of the brain using a full-field laser perfusion imager (RFLS III) in accordance with the manufacturer's instructions (RWD Life Science, Shenzhen, China). The mice were subjected to CA as previously described. Furthermore, a midline scalp incision was made to expose the skull for laser speckle imaging, with the imager positioned directly over the skull. A laser diode emitting at 785 nm was utilized to illuminate the skull surface, enabling the laser to penetrate the brain in a diffused manner. Cerebral blood flow was measured using speckle contrast. The following imaging parameters were used: spatial filter constant of 3 s, camera frame rate of 50 fps, and resolution of 2048×2048.

2.7 | Label dying cells in vivo

The PS redistribution to the external surface of plasma membrane is central to recognition of apoptotic cell and serves as a molecular cue for phagocyte engulfment, such as microglia. Annexin V is highly affinitive to PS and can serve as a sensitive probe to detect externalized PS. Therefore, we labeled apoptotic cell in vivo with Annexin V-EGFP Apoptosis Detection Kit (CX005S, EpiZyme Biotech, Shanghai, China) by i.c.m. administration of 5 µL 2 h before sacrificing the mice.

2.8 | RNA preparation and qPCR

The isolation of total RNA was conducted on murine brain tissue employing a kit designed for the purification of total RNA from animal tissues (RE-03014, FORE-GENE, Chengdu, China). Reverse transcription of RNA

to cDNA was achieved using HiScript III RT SuperMix for quantitative PCR, in conjunction with a genomic DNA (gDNA) wiper (R322, Vazyme, Nanjing, China). qPCR was then performed by ChamQ Universal SYBR qPCR Master Mix (Q711, Vazyme, Nanjing, China) using a Roche LightCycler 480 System to measure the mRNA expression of MFG-E8 and β-actin. Relative changes of mRNA expressions were normalized by the expression levels of β-actin. Primer sequences for qPCR are available in Table S1.

2.9 | Western blot

Western blotting was performed routinely as previously reported [25]. Briefly, brain tissues were rapidly dissected on ice and placed in RIPA lysis buffer (Beyotime, Shanghai, China) containing a protease inhibitor cocktail and phosphatase inhibitor (Beyotime, Shanghai, China). Denatured proteins in the SDS loading buffer were separated on SDS-PAGE gels and transferred to polyvinylidene difluoride membranes (Millipore, Billerica, USA). The transmembrane efficiency and the total amount of proteins sampled in each well were verified by No-Stain™ Protein Labeling Reagent (Invitrogen, Waltham, USA). After blocking, the membranes were incubated overnight at 4°C with primary antibodies anti-IRF7 (1:1000, 22392-1-AP, Proteintech, Wuhan, China). After washing with TBST, the membranes were incubated with HRP-conjugated secondary antibodies (Beyotime, Shanghai, China), and the bands were detected using enhanced chemiluminescence advanced Western blotting detection reagents (P10100, NCM Biotech, Suzhou, China). Protein band intensities were quantified and normalized to the level of total protein using ImageJ software.

2.10 | Histological examination

Mice were euthanized after behavior tests or at predetermined time points, and 5 μm coronal brain paraffin sections (Leica Biosystems RM2245, Heidelberg, Germany) and 50 μm frozen sections (Leica CM1950, Leica Microsystems GmbH, Heidelberg, Germany) were obtained. To ascertain the extent of neuronal loss, sections of the brain were subjected to Nissl staining (Beyotime, Shanghai, China) and observed under a microscope (Pannoramic MIDI, 3D Histech Digital Pathology System, Jinan, China). Viable neurons in the cortex and hippocampal CA1 region were identified as those exhibiting visible nuclei, intact cytoplasm, and numerous Nissl bodies. Conversely, neurons exhibiting shrunken cell bodies surrounded by empty space and sparse Nissl bodies were considered to be damaged or dead neurons.

And the immunofluorescence method was employed, with brain sections incubated with the following primary antibodies: anti-Iba1 antibody (1:5000, ab283319,

Abcam, Cambridge, UK), anti-EGFP antibody (1:500, T61602, Abmart, Shanghai, China), anti-His-Tag antibody (1:100, TT0009, Abmart, Shanghai, China), anti-Arg1 antibody (1:100, ab233548, Abcam, Cambridge, UK), anti-iNOS antibody (1:100, ab178945, Abcam, Cambridge, UK), anti-NeuN antibody (1:500, 94403S, CST, Boston, USA), anti-GFAP antibody (1:500, ab190288, Abcam, Cambridge, UK), and anti-MAP2 antibody (1:10000, ab5392, Abcam, Cambridge, UK). Subsequently, the sections were washed and detected with the appropriate Alexa Fluor secondary antibody, followed by DAPI counterstaining in the dark. Immunofluorescence signaling was then observed with an inverted fluorescence microscope (Olympus IX73, Tokyo, Japan), and at least 3 slide fields were randomly obtained in each brain section, and 3D images were obtained via confocal microscopy (LSM980, Zeiss, Oberkochen, Germany). The relative area of MAP2 immunoreactivity in the cortex and hippocampal CA1 region and the number of cells showing immunoreactivity for the other molecular markers listed above were quantified by an investigator unknown to experimental grouping by Image J software (NIH).

2.11 | Flow cytometry analysis and sorting

The flow cytometry was performed as previously described with some modifications [26]. The CD11b$^+$/CD45^{med} was chosen to categorize microglia in this study (Figure S3) because the expression level of CD45 increases under injury conditions [27]. A total of 54 mice were used to extract microglial cells, with 6 mice combined into one sample and 3 samples per group. Briefly, on the 3rd day post-ROSC, the entire brain tissue was harvested and mechanically dissociated and placed in a 1.5 mL EP tube containing digestion solution. The mixture was then incubated for 40 min at 37°C. A single-cell suspension was then prepared using a 70-μm cell strainer.

The isolation of cells was achieved by centrifugation using a 33% Percoll gradient solution, followed by washing and resuspension in phosphate-buffered saline (PBS) containing 2% bovine serum albumin (BSA). Subsequently, the samples were incubated with the following antibodies for 30 min at 4°C: FITC-conjugated CD11b, APC-conjugated CD45, and 7-AAD (BD Biosciences, New Jersey, USA), in the presence of Fc-block CD16/32 (BD Biosciences, New Jersey, USA) to prevent non-specific binding. The population of microglia (CD11b$^+$/CD45^{med}) was sorted using an ultra-fast flow cell sorting system. The detailed process was shown in Data S1.

2.12 | RNA sequencing and data analysis

Total RNA of microglia was harvested with TRIzol in accordance with the manufacturer's protocol (Novogene, Beijing, China). The mRNA fragments after assessed and

purified were reverse transcribed into cDNA and amplified by PCR. Subsequently, the PCR reaction was purified and the quality of the DNA library was assessed. Finally, clustering of the indexed samples was performed on a cBot Cluster Generation System (Illumina) according to the manufacturer's instructions. After clustering, the library preparations were sequenced on an Illumina Novaseq 6000 and 150 bp paired-end reads were generated.

Fragments per Kilobase of transcript per Million mapped reads (FPKM) were used for gene expression and were $\log2(x + 1)$ transformed. Genes with p-value <0.05 found by DESeq2 were designated as differentially expressed. Gene Ontology (GO) enrichment analysis of differentially expressed genes (DEGs) was performed using the Cluster Profiler R package. Gene Ontology (GO) terms with fold change >2 or <−2 and a p-value <0.05 were considered significantly enriched for DEGs. R package pheatmap was used to generate heatmap. The detailed process was illustrated in Data S1.

2.13 | RNA interference

Mice were transfected with small interfering RNA (siRNA) directed against IRF7 or scrambled siRNA (ChemShine Biotechnology, Shanghai, China) with in vivo transfection reagent (101000040, Polyplus, Strasbourg, France) in accordance with the manufacturer's instructions. In brief, siRNA and transfection reagent were diluted in 10% glucose solution, mixed, incubated for 15 min at room temperature, and 5 μL of the complex was injected intracerebroventricularly (icv) into mice. The sequences of scrambled siRNA were (F) UUCUCC-GAACGUGUCACGUdTdT, (R) ACGUGACACGU UCGGAGAAdTdT. The sequences of IRF7 siRNA were (F) GAAGAGGCUGGAAGACCAAdTdT, (R) UUGGUCUUCCAGCCUCUUCdTdT.

2.14 | Statistical analysis

All continuously distributed variables were reported as means ± standard deviations (SD), as indicated in the corresponding legends. Student's t-test was used to compare data between two groups, while one-way ANOVA followed by Tukey's post hoc multiple testing was used to compare data among multiple groups. Kaplan–Meier analysis with log-rank test was used to measure survival difference. Mann–Whitney U test or Kruskal–Wallis test with Dunn's multiple comparison test were performed to compare neurological function scores. The analysis of escape latency data from water maze training involved the use of a repeated-measures ANOVA, with the factors of treatment group, time point, and the interaction between treatment and time point. The analysis was followed by the application of Tukey's post hoc multiple comparison tests. The data were analyzed statistically with the aid of GraphPad Prism, Version 9.5, and SPSS 20.0 (IBM, Armonk, NY). A two-tailed p-value of less than 0.05 was considered statistically significant.

2.15 | Role of funders

The funders of this study did not play a role in the study design, data collection, data analyses, interpretation, or the writing of this manuscript.

3 | RESULTS

### 3.1 | rmMFG-E8 administration enhances the microglial efferocytosis of apoptotic cells after CA/CPR

We first determined whether a supplement of rmMFG-E8 enhanced efferocytosis of apoptotic cells by microglia after CA/CPR in mice. We labeled rmMFG-E8 with His-Tag and microglia/macrophages (for convenience, microglia were used in the following text) with Iba-1 at 12 h after CA/CPR (Figure S4). His-Tag$^+$ cells were observed only in the rmMFG-E8 group. Iba-1$^+$ microglia contacted and wrapped around His-Tag$^+$, neuron-like cells in the cortex, and hippocampal CA1 region in the rmMFG-E8 group, indicating that rmMFG-E8 was successfully delivered to the brain and might act as a bridging molecule mediating the recognition of injured cells by microglia [15].

To confirm the above suspicion, we labeled PS-inverted apoptotic cells with Annexin V-EGFP and microglia with Iba-1 after CA/CPR or sham operation in mice (Figure 1A). As illustrated, the efferocytosis of apoptotic cells could be divided into four stages: non-touching, touching, enwrapping, and engulfing, among which the latter three stages were counted as phagocytosis of dying cells by microglia in this study (Figure 1B) [28]. Three-dimensional stereoscopic images captured using confocal microscopy further confirmed the phagocytosis of apoptotic cells by microglia (Figure 1C). Sham-operated mice exhibited a rare number of PS eversion cells (Figure 1D) and were thus excluded from the statistical analysis. By contrast, CA/CPR caused extensive apoptotic cells with exposed PS (Annexin V$^+$) in the cortex on the 1st, 3rd, and 7th day (Figure 1D,F). Compared with vehicle treatment, rmMFG-E8 treatment remarkably increased the number of microglia on the 3rd day and 7th day after CA/CPR (Figure 1D,E), which may be related to the pro-proliferation of rmMFG-E8 [29, 30] and efferocytosis-induced microglia proliferation [31]. Besides, rmMFG-E8 administration led to an increased number of apoptotic cells phagocytosed by microglia and a higher

phagocytosis index on the 3rd day (Figure 1G,H). Moreover, the number of apoptotic cells on the 7th day was significantly reduced after rmMFG-E8 treatment (Figure 1F). These data suggest that rmMFG-E8 administration enhances efferocytosis of apoptotic cells by microglia and activates continuous efferocytosis to prevent secondary necrosis of injured cells after CA/CPR [32].

3.2 | rmMFG-E8 administration improves survival and neurological outcomes after CA/CPR

The accumulation of apoptotic cells triggers neuroinflammation, leading to more cell death, and creating a vicious cycle [33], whereas enhancing microglial efferocytosis of
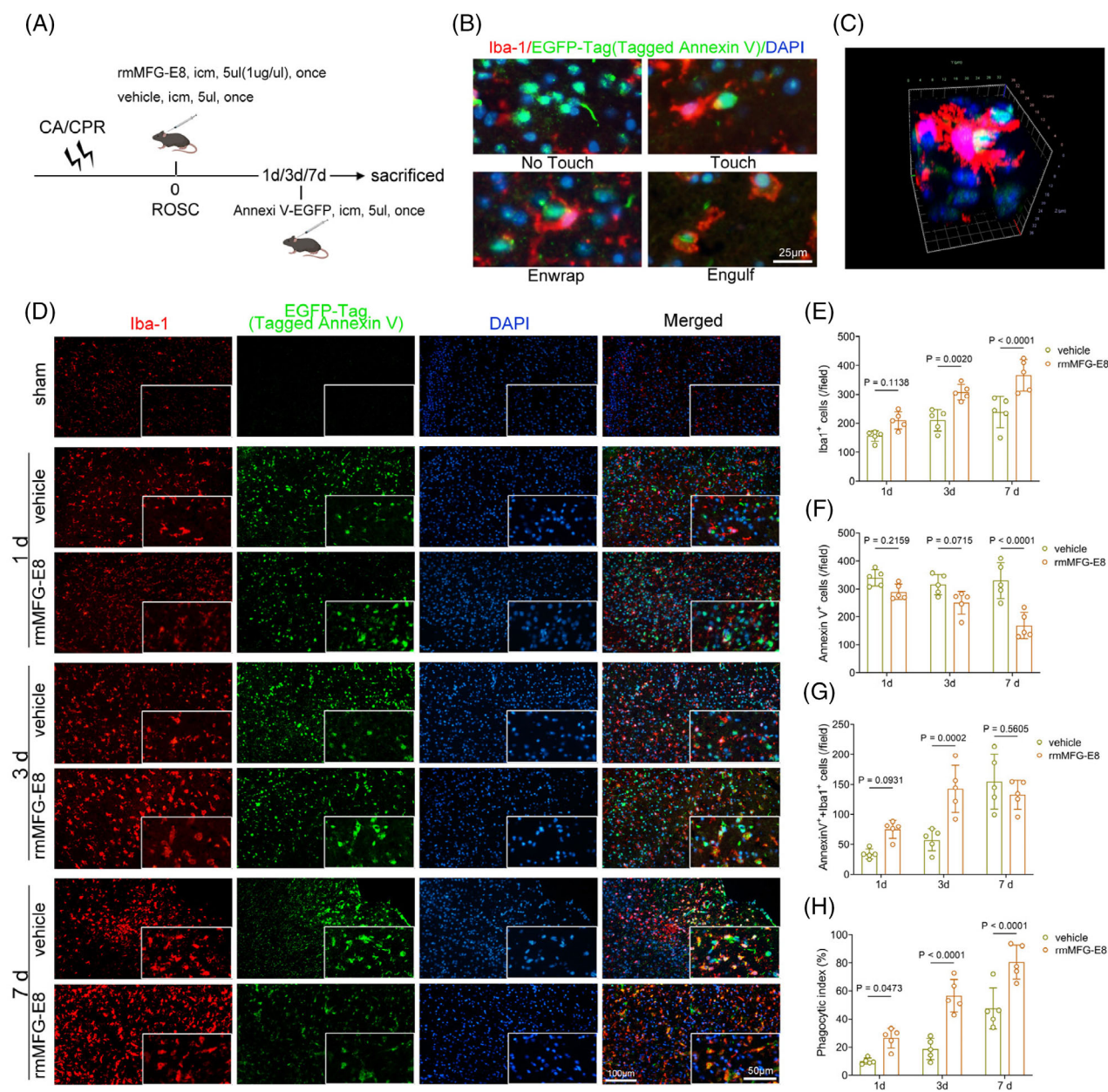
FIGURE 1 Effects of recombinant mouse MFG-E8 (rmMFG-E8) on microglia-mediated efferocytosis after cardiac arrest and cardiopulmonary resuscitation (CA/CPR). A. Experimental procedures of this part. B. The zooming images represent four stages of efferocytosis: Non-touching, touching, enwrapping, and engulfing. Scale bar: 25 μm. C. Phosphatidylserine (PS)-eversion-cell engulfed by microglia was observed with a confocal microscope. D. Double immunofluorescence labeling for enhanced green fluorescent protein (EGFP)-Tagged Annexin V (green), Iba1 (red), and 4,6-diamidino-2-phenylindole (DAPI) (blue) at 1d/3d/7d after CA/CPR. Scale bar: 50 or 100 μm. E. Microglia (Iba1$^+$) in each group after CA/CPR. F. Cells with PS eversion at 1d/3d/7d of the two groups. G. PS eversion cells involved in phagocytosis (AnnexinV$^+$Iba1$^+$) at 1d/3d/7d after CA/CPR. H. The phagocytosis index represented by AnnexinV$^+$Iba1$^+$/AnnexinV$^+$ × 100% in the two groups. i.c.m., intra-cisterna magna injection; ROSC, return of spontaneous circulation.
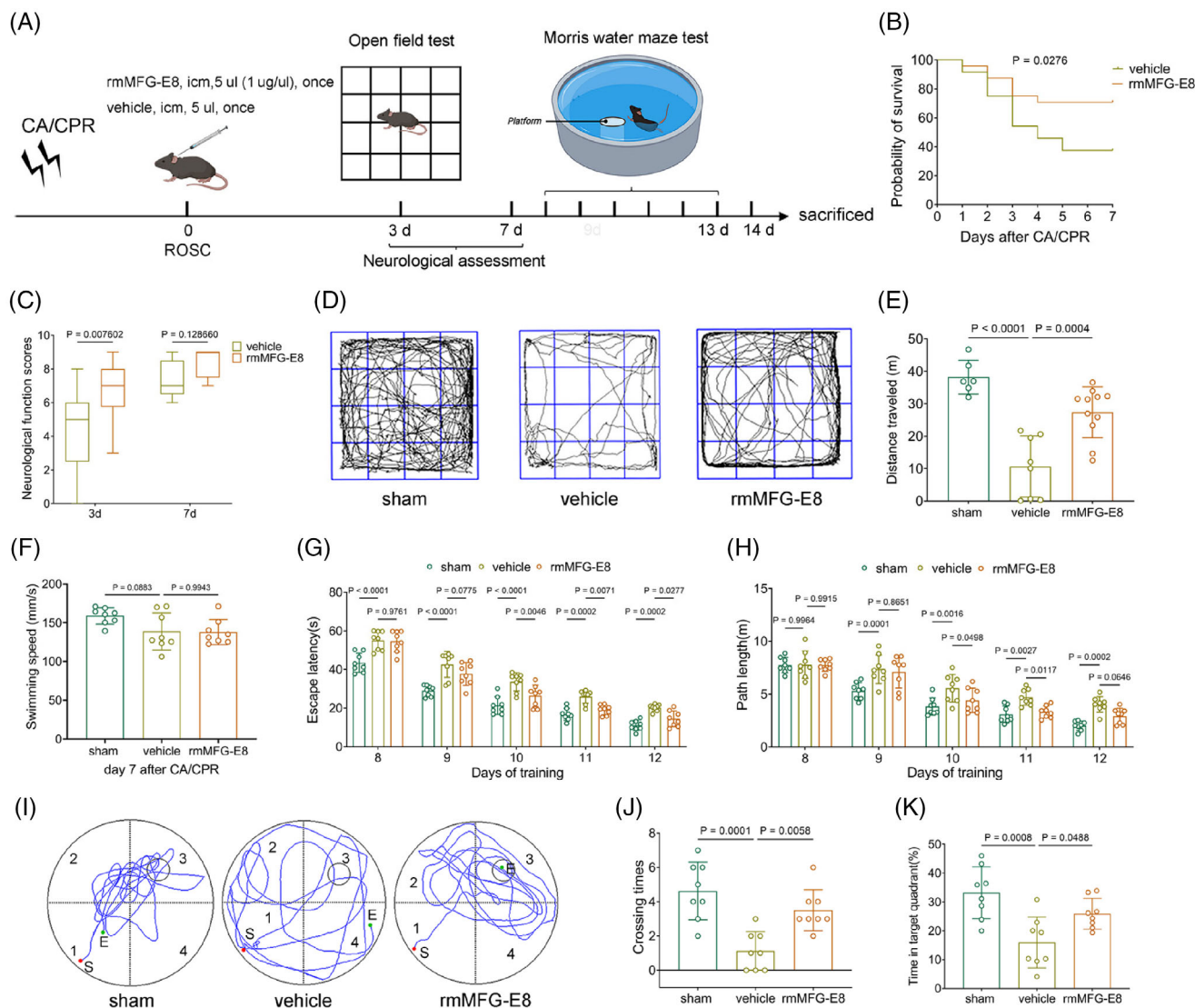
FIGURE 2 Effects of recombinant mouse MFG-E8 (rmMFG-E8) on survival and neurological function after cardiac arrest and cardiopulmonary resuscitation (CA/CPR). A. Experimental procedures of this part. B. The cumulative survival during the 7-day follow-up after return of spontaneous circulation (ROSC), vehicle group (n = 24), rmMFG-E8 group (n = 24). C. The neurological function scores of survived mice on the 3rd day and 7th day after ROSC. The 3rd day, vehicle group (n = 13), rmMFG-E8 group (n = 18); the 7th day, vehicle group (n = 9), rmMFG-E8 group (n = 17). D. Representative tracks of mice in different groups during the open field test. E. The total distance traveled in the open field test among three groups. F. Average swimming speed in the Morris water maze test on the 7th day after surgery or ROSC. G. The escape latency of mice in different groups to find the platform in Morris water maze test. H. The swimming path length of mice during spatial exploration experiment. I. Representative swimming tracks of mice during the probe trial, S, start; E, end. J, K. The crossing times and the percentage of time in the target quadrant during the probe trial. i.c.m., intra-cisterna magna injection.

apoptotic cells may be beneficial in attenuating histological injury [34]. The efferocytosis of apoptotic cells may also enable microglia to initiate an anti-inflammatory pathway, preventing neuroinflammation progression and maintaining brain homeostasis [9]. Therefore, we explored whether the enhanced efferocytosis by rmMFG-E8 treatment could lead to improved survival and neurological function in mice after CA/CPR (Figure 2A). No significant differences in body weight, time from asphyxia to CA, time required for ROSC, the total epinephrine dose, MAP, HR, and rectal temperature were found between the vehicle and rmMFG-E8 groups (Table S2).

The survival rate of mice in the rmMFG-E8 group was 70.83% (17 of 24), which was significantly higher than the 37.5% (9 of 24) in the vehicle group (Figure 2B) in the 7-day survival observation after CA/CPR. Additionally, a 9-score neurological function scoring system was used to assess neurological deficiency on the 3rd day, 7th day, and 14th day after CA/CPR and the results demonstrated that rmMFG-E8-treated mice exhibited statistically better neurological function scores on the 3rd day after ROSC (Figure 2C). However, there was no apparent difference in neurological scores on the 7th day and 14th day between the vehicle and rmMFG-E8 groups (Figure 2C,

Figure S2B), possibly because the more severely neurologically impaired animals in the vehicle group had died before the 7th day after ROSC. Subsequently, the open field test was performed to evaluate the gross motor function and general activity of the mice on the 3rd day after CA/CPR (Figure 2D). The analyzed results showed that the post-CA/CPR mice in the rmMFG-E8 group traveled faster and had a longer distance than those in the vehicle group (Figure S2A, Figure 2E).

The Morris water maze test was also used to access the effect of rmMFG-E8 on short-term spatial learning and memory abilities after CA/CPR. The average swimming speeds of surviving mice were assessed to exclude the interference of discrepant swimming speeds on the escape latency on the 7th day (Figure 2F). Mice in the sham, vehicle, and rmMFG-E8 groups all showed a gradual decrease in escape latency ($F = 243.1$, $p < 0.0001$) to find the hidden platform during hidden platform training from the 8th day to 12th day after surgery or CA/CPR. In addition, the analysis of training data using repeated-measures ANOVA revealed a significant difference in escape latency among the groups ($F = 63.34$, $p < 0.0001$), with no significant interaction between groups and time points ($F = 1.675$, $p = 0.113$). Compared with the sham operation, CA/CPR led to increased latencies from the 8th day to 12th day in the vehicle group (all $p < 0.001$ vs. sham). By contrast, the extended latencies were partly terminated by rmMFG-E8 treatment from the 10th day to 12th day (all $p < 0.05$ vs. vehicle) (Figure 2G, Figure S2C). The mice in the vehicle group had a longer swimming path length than that in the sham group from the 9th day to 12th day (all $p < 0.01$ vs. sham), whereas rmMFG-E8 treatment significantly shortened swimming distances to find the hidden platform on the 10th day and 11th day (all $p < 0.05$ vs. vehicle) (Figure 2H).

The probe test to assess short-term memory was performed on all mice on the 13th day after CA/CPR (Figure 2I). The results showed that the frequency of vehicle group crossing the platform was less than the sham group, while the rmMFG-E8 group reversed this trend (Figure 2J). Moreover, rmMFG-E8-treated mice spent significantly more time searching the platform quadrant (Q3) compared with vehicle-treated mice, which spent much time searching the other three non-platform quadrants (Figure 2K). These findings suggest that rmMFG-E8 treatment partly rescues CA/CPR-induced spatial learning and memory deficits.

Taken together, these results demonstrate that rmMFG-E8 treatment after CA/CPR improves 7-day survival rate and neurological outcomes.

3.3 | rmMFG-E8 administration alleviates neuronal loss and glial activation after CA/CPR

Post-ischemic reperfusion is followed by great hippocampal neuronal death and cellular inflammatory reactions [35–37]. Thus, Nissl staining and immunofluorescence were performed on brain sections from mice sacrificed on the 14th day to observe differences in histological damage among the different groups (Figure 3A–C). The results showed that the number of viable neurons stained by Nissl and NeuN was significantly decreased in the vehicle group compared with the sham group, and rmMFG-E8 treatment markedly suppressed neuronal loss (Figure 3F,G). Furthermore, CA/CPR induced extensive damage to neuronal dendrites, as indicated by decreased MAP-2 immunostaining compared to the sham group, and this dendritic damage was partly attenuated by rmMFG-E8 treatment (Figure 3C,H).

Microglia and astrocytes, as the prominent innate immune cells, play a vital role in coordinating neuroinflammatory responses [38–40], which are activated and migrate to the injury sites after CA/CPR [26, 41]. In our study, more Iba1-positive microglia and GFAP-positive astrocytes were detected in the vehicle group than in the sham group, indicating that CA/CPR exacerbated neuroinflammation (Figure 3D,E). In comparison, rmMFG-E8-treated mice showed a remarkable reduction in glial activation (Figure 3I,J). Collectively, these findings demonstrate that rmMFG-E8 treatment substantially alleviates histological damage and inflammatory reactions in post-CA/CPR mice.

3.4 | rmMFG-E8 administration promotes microglia to switch to an anti-inflammatory phenotype

The efferocytosis of apoptotic cells by phagocytes prevents the secondary necrosis of apoptotic cells and allows the phagocytes to switch to an anti-inflammatory phenotype [42]. To investigate the functional status of microglia in rmMFG-E8-treated mice after CA/CPR, we co-labelled the proinflammatory marker iNOS and the anti-inflammatory marker Arg1 with Iba1 (Figure 4A). Since the PS-inverted cells involved in phagocytosis of microglia in rmMFG-E8 group was significantly higher than vehicle group on the 3rd day after CA/CPR, we chose this time point for the following analysis. The percentage of iNOS and Iba1 double-positive microglia was significantly elevated in the vehicle group after CA/CPR but decreased in the rmMFG-E8 group (Figure 4B,D). By contrast, the percentage of microglia that were double-positive for Arg1 and Iba1 was significantly higher in the rmMFG-E8 group (Figure 4C,E). We next performed PCR for proinflammatory and anti-inflammatory markers following rmMFG-E8 injection and IRF7 silencing. The qPCR analysis demonstrated that the expression of anti-inflammatory markers, including Il-10 and Il-4, was dramatically up-regulated (Figure 4F,G), while the expression of proinflammatory markers, such as Il-1β, Il-6, and TNF-α, was obviously reduced following rmMFG-E8 administration (Figure 4H–J). These data indicate that rmMFG-E8 treatment promotes microglia to switch to an anti-inflammatory phenotype and relieves inflammatory response after CA/CPR.
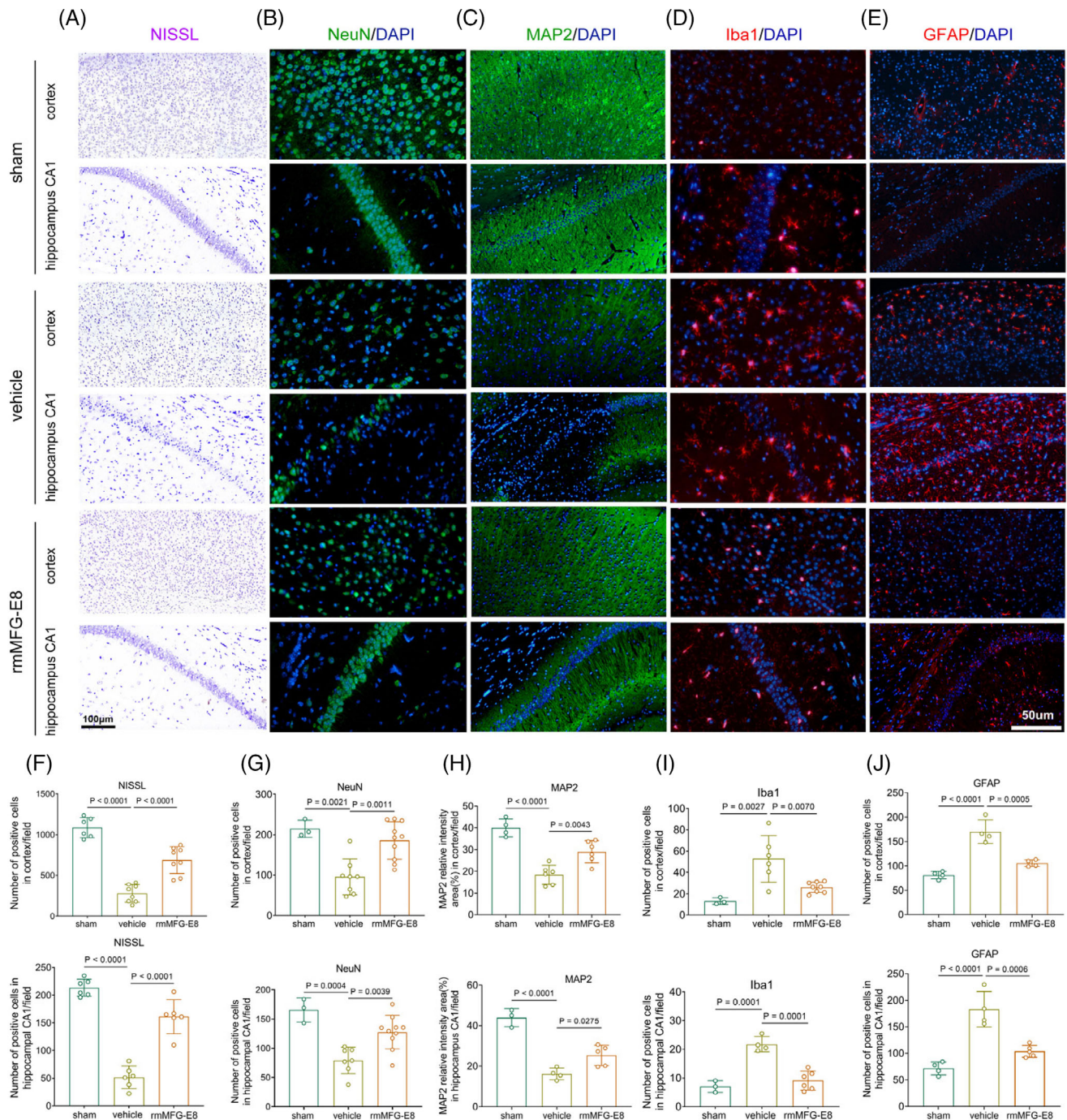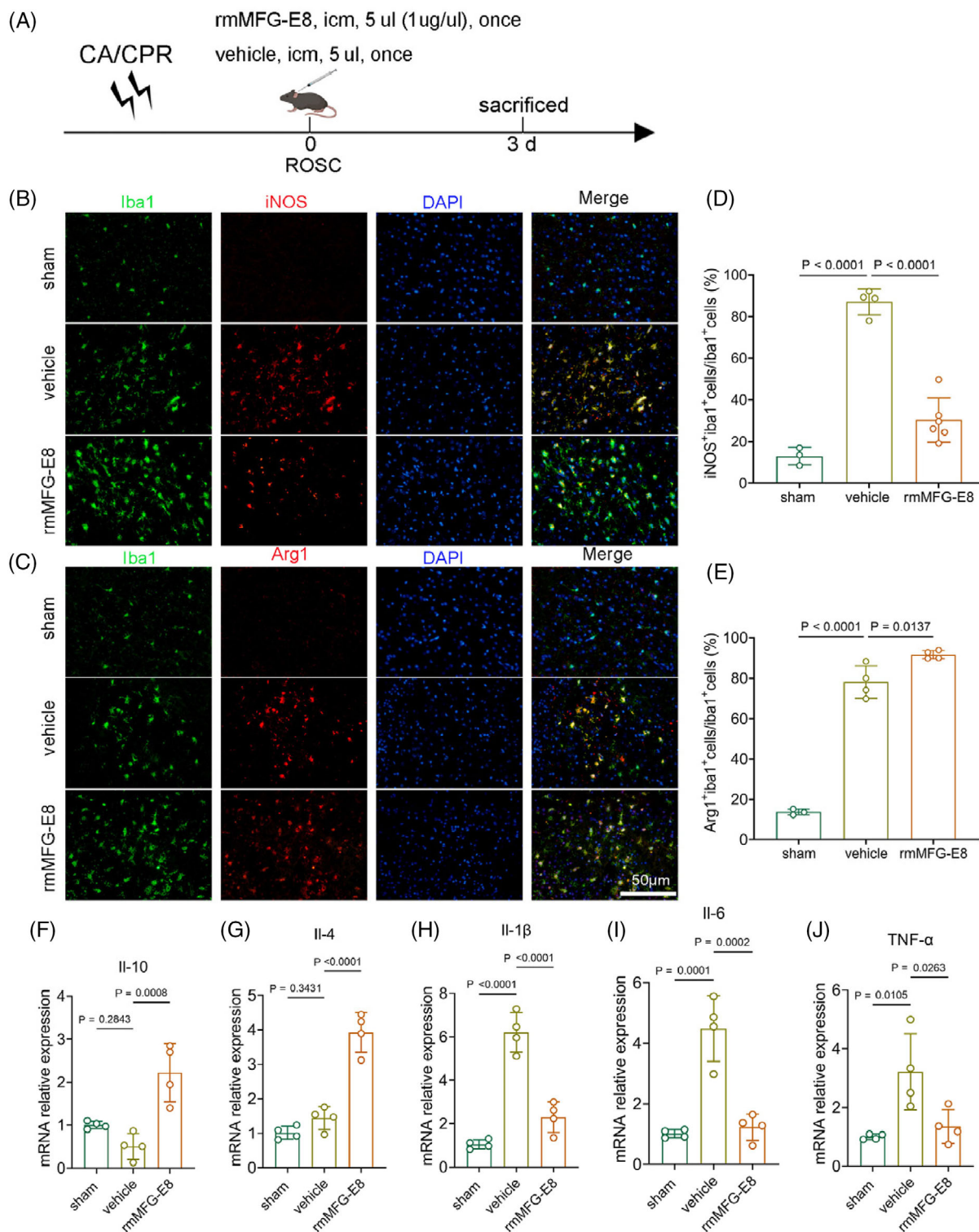
FIGURE 3 Effects of recombinant mouse MFG-E8 (rmMFG-E8) on neuropathological damage and glial activation after cardiac arrest and cardiopulmonary resuscitation (CA/CPR). A. Representative photomicrographs of post-CA/CPR neuropathological damage characterized by Nissl staining (purple) in the cerebral cortex and hippocampal CA1 region of the sham group and the experimental groups on the 14th day after return of spontaneous circulation. Scale bar, 100 μm. B–E. Immunofluorescence staining for NeuN (green), MAP2 (green), Iba1 (red), and Glial fibrillary acidic protein (GFAP) (red) in the cerebral cortex and hippocampal CA1 region. Nuclei are visualized with 4,6-diamidino-2-phenylindole (DAPI) stain (blue). Scale bar, 50 μm. F–J. Quantification results of Nissl, NeuN, MAP2, Iba1, and GFAP staining in the cerebral cortex and hippocampal CA1 region.

3.5 | rmMFG-E8 administration induces a prominent alteration in microglial gene expression after CA/CPR

To elucidate the molecular events elicited by MFG-E8 administration after CA/CPR, FACS was performed to isolate the microglia population (CD11b$^+$/CD45^{med}) from the brain tissue on the 3rd day after CA/CPR or sham operation. Microglia sorted from sham, vehicle, and rmMFG-E8 groups were subjected to bulk RNA-seq (Figure 5A). To determine the transcriptomic changes of microglia induced by CA/CPR, we performed differential

FIGURE 4 Effects of recombinant mouse MFG-E8 (rmMFG-E8) on microglia polarization and inflammation response after cardiac arrest and cardiopulmonary resuscitation (CA/CPR). A. Experimental procedures of this part. B, C. Immunofluorescence staining on the 3rd day after CA/CPR with Iba1(green), iNOS (red) as a marker of a proinflammatory phenotype of microglia, and Arg1 (red) representing an anti-inflammatory phenotype of microglia. Scale bar: 50 μm. D, E. Quantification of the percentage of iNOS and Iba1 double-positive cells, and Arg1 and Iba1 double-positive cells, respectively. F–J. qPCR analysis of proinflammatory and anti-inflammatory markers expression following rmMFG-E8 administration. DAPI, 4,6-diamidino-2-phenylindole; i.c.m, intra-cisterna magna injection; ROSC, return of spontaneous circulation.
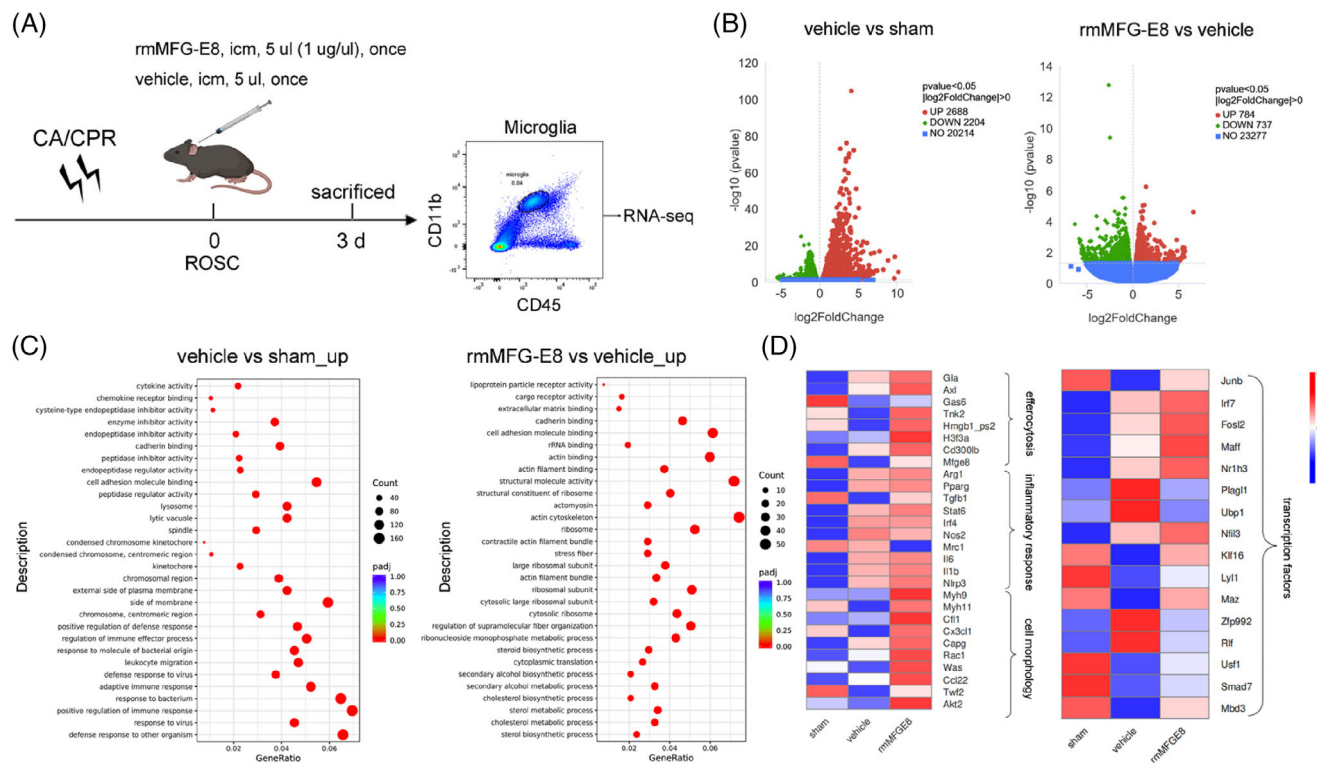
FIGURE 5 Effects of recombinant mouse MFG-E8 (rmMFG-E8) on microglial transcriptomic alterations after cardiac arrest and cardiopulmonary resuscitation (CA/CPR). A. Experimental procedures of this part. B. Volcano plots display the number of up- and down-regulated differentially expressed genes (DEGs) in microglia among different groups. C. Pathway enrichment plots show significantly overrepresented gene ontology terms and 30 major functional clusters were identified (amplified pictures in Figure S5). D. Left panel: RNA-seq expression profile of DEGs involved in efferocytosis, inflammatory response, and cell morphology. Right panel: RNA-seq expression profile of transcription factor DEGs (amplified pictures in Figure S6). i.c.m., intra-cisterna magna injection; ROSC, return of spontaneous circulation; red□high relative expression; white□mean expression; blue□low relative expression.

expression analysis. The volcano diagrams indicated that a total of 4892 genes were identified as DEGs, which contained 2688 up-regulated genes and 2204 down-regulated genes in the vehicle group compared with the sham group (Figure 5B, left), indicating the substantial alterations of the transcriptome (about 19.73% of total genes). In parallel, the same analysis was performed to determine the transcriptomic changes of microglia from rmMFG-E8-treated mice after CA/CPR. A total of 1521 genes were identified as DEGs, which contained 784 up-regulated genes and 737 down-regulated genes in the rmMFG-E8 group compared with the vehicle group (Figure 5B, right), indicating significant alterations of the transcriptome (about 6.13% of total genes).

To clarify the functional changes in post-CA/CPR microglia after rmMFG-E8 administration, we performed pathway enrichment analysis on the DEGs using the online tool Metascape. The GO terms obtained from Metascape showed that regulation of cell adhesion, immune response, defense response, and membrane changes accounted for a significant proportion of the differences between the sham and vehicle groups (Figure 5C, left). The comparison between the vehicle and rmMFG-E8 groups revealed a significant difference

in the regulation of cell adhesion, structural molecule activity, actin binding, and actin cytoskeleton (Figure 5C, right).

We then focused on genes related to efferocytosis, inflammatory response, cell morphology, and transcription regulation. The heatmap showed that 8 efferocytosis-related genes (*Gla*, *Axl*, *Gas6*, *Tnk2*, *Hmgb1_ps2*, *H3f3a*, *Cd300lb*, *Mfge8*), 10 inflammatory response-related genes (*Arg1*, *Pparg*, *Tgfb1*, *Stat6*, *Irf4*, *Nos2*, *Mrc1*, *Il6*, *Il1b*, *Nlrp3*), and 10 cell morphology-related genes (*Myh9*, *Myh11*, *Cfl1*, *Cx3cl1*, *Capg*, *Rac1*, *Was*, *Ccl22*, *Twf2*, *Akt2*) were involved (Figure 5D, left).

Efferocytosis-associated genes, including *Gla*, *Axl*, *Tnk2*, *Hmgb1_ps2*, *H3f3a*, *Cd300lb*, and *Mfge8*, were up-regulated in rmMFG-E8 group. Genes associated with microglia anti-inflammatory phenotypes, such as *Arg1*, tended to up-regulate, and genes associated with microglia proinflammatory phenotypes, such as *Nos2*, tended to down-regulate after rmMFG-E8 administration compared with vehicle administration. These data indicate that a variety of genes were changed in post-CA/CPR microglia treated with rmMFG-E8, including efferocytosis-related bridging, membrane receptors, complements, morphology-related myosin, chemokines, and

inflammatory cytokines, to remove the dying cells and modulate the inflammatory response.

To explore the underlying mechanism by which rmMFG-E8 drives the transformation of microglia from a proinflammatory to an anti-inflammatory phenotype, we screened DEGs intersections among 3 compared groups (vehicle vs. sham, rmMFG-E8 vs. vehicle, rmMFG-E8 vs. sham) and identified *Irf7*, *Dusp5*, *Ifi2712a*, *Tgfbi*, and *Igals3*. We further screened transcription factors intersected between vehicle vs. sham and rmMFG-E8 vs. vehicle and identified *Junb*, *Irf7*, *Fosl2*, *Maff*, *Nr1h3*, *Plagl1*, *Ubp1*, *Nfil3*, *Klf16*, *Lyl1*, *Maz*, *Zfp992*, *Rlf*, *Usf1*, *Smad7*, and *Mbd3* (Figure 5D, right). Among these screened DEGs and transcription factors, we identified IRF7, an essential transcription factor for immune responses [43], whose involvement in the switch of proinflammatory to anti-inflammatory phenotype has been reported in myeloid cells [44]. The induction of IRF7 expression improves the resolution of proinflammatory cytokines and leads to anti-inflammatory conversion of microglia after spinal cord injury [44], and the IRF7 up-regulation also has neuroprotective effects in mice with postoperative neurocognitive impairment [45]. Therefore, we speculate that IRF7 might be involved in converting microglia to an anti-inflammatory phenotype after MFG-E8 administration.

## 3.6 | IRF7 mediates the neuroprotective effects of rmMFG-E8 administration after CA/CPR

To confirm the role of IRF7 in rmMFG-E8-mediated neuroprotective effects and microglial polarization towards an anti-inflammatory phenotype, we first used qPCR to access IRF7 expression. The results indicated that IRF7 expression was up-regulated in microglia on the 3rd day after CA/CPR in the rmMFG-E8 group compared with the vehicle group (Figure 6A). Furthermore, we used adeno-associated virus (AAV)-mediated shRNA delivery strategy targeting microglia to knock down IRF7, while the transfection efficiency and specificity of these AAV variants are unsatisfactory (Figure S7). Therefore, we selected suitable siRNAs for silencing IRF7 and verified their silence efficiency by qPCR and Western blot, which showed IRF7 siRNA3 had effective silence efficiency (Figure 6B–D). Therefore, we used IRF7 siRNA3 for the subsequent experiments. No significant differences in body weight, time from asphyxia to CA, time required for ROSC, the total epinephrine dose, MAP, HR, and rectal temperature were found among scrambled siRNA, rmMFG-E8 + scramble siRNA, and rmMFG-E8 + IRF7 siRNA groups (Table S3).

First, we silenced IRF7 expression in the mouse brain using effective siRNA and then examined the effects of rmMFG-E8 on neurological outcomes (Figure 6E). Scrambled siRNA, rmMFG-E8 + scramble siRNA, and rmMFG-E8 + IRF7 siRNA were injected via the lateral ventricle immediately after CA/CPR. Next, neurological function tests were performed on each group of mice on the 3rd day, 7th day, and 14th day after CA/CPR. The results of the neurological function assessment indicated that mice in the rmMFG-E8 + scrambled siRNA group had higher total scores than those in the scrambled siRNA group on the 3rd day following ROSC, while the total scores of mice in the rmMFG-E8 + IRF7 siRNA group were lower than those in the rmMFG-E8 + scrambled siRNA group (Figure 6F). However, there is no significant difference in the neurological function assessment among the three groups on the 7th day and 14th day after CA/CPR (Figure 6F, Figure S8B), possibly because the more severely neurologically impaired mice had died before the 7th day post-CA. Concerning open field test, the mice in the scramble siRNA group moved slower and had shorter distances compared with the sham-operated group, while mice in the rmMFG-E8 + scrambled siRNA group moved faster and had longer distances than those in the scrambled siRNA group (Figure 6G,H, Figure S8A). However, the mice in the rmMFG-E8 + IRF7 siRNA group exhibited a reduction of movement speed and distance compared with the rmMFG-E8 + scrambled siRNA group (Figure 6G,H, Figure S8A). Subsequently, the Morris water maze test was also used to access the effect of IRF7 silence in rmMFG-E8 mediated short-term spatial learning and memory abilities after CA/CPR. The average swimming speeds of surviving mice were assessed to exclude the interference of discrepant swimming speeds on the escape latency on the 7th day (Figure 6I). Mice in the sham, scrambled siRNA, rmMFG-E8 + scramble siRNA, and rmMFG-E8 + IRF7 siRNA groups all showed a gradual decrease in escape latency ($F = 332.1$, $p < 0.0001$) to find the hidden platform during hidden platform training from the 8th day to 12th day after surgery or CA/CPR. Additionally, the training data analysis using repeated-measures ANOVA revealed a significant difference in escape latency among the groups ($F = 80.59$, $p < 0.0001$), with no significant interaction between groups and time points ($F = 1.847$, $p = 0.0518$). Consistent with previous results, CA/CPR led to increased latencies from the 8th day to 12th day in the scrambled siRNA group (all $p < 0.01$ vs. sham) compared with the sham operation, while the extended latencies were partly terminated by rmMFG-E8 + scrambled siRNA treatment from the 9th day to 12th day (all $p < 0.001$ vs. scrambled siRNA) (Figure 6J, Figure S8C). By contrast, the latencies were significantly increased in rmMFG-E8 + IRF7 siRNA group compared with rmMFG-E8 + scrambled siRNA group from the 9th day to 12th day (all $p < 0.05$ vs. rmMFG-E8 + scrambled siRNA) (Figure 6J, Figure S8C). The mice in the scrambled siRNA group had a longer swimming path length than that in the sham group on the 9th, 10th, and 12th day ($p < 0.01$ vs. sham), whereas rmMFG-E8 + scrambled siRNA treatment
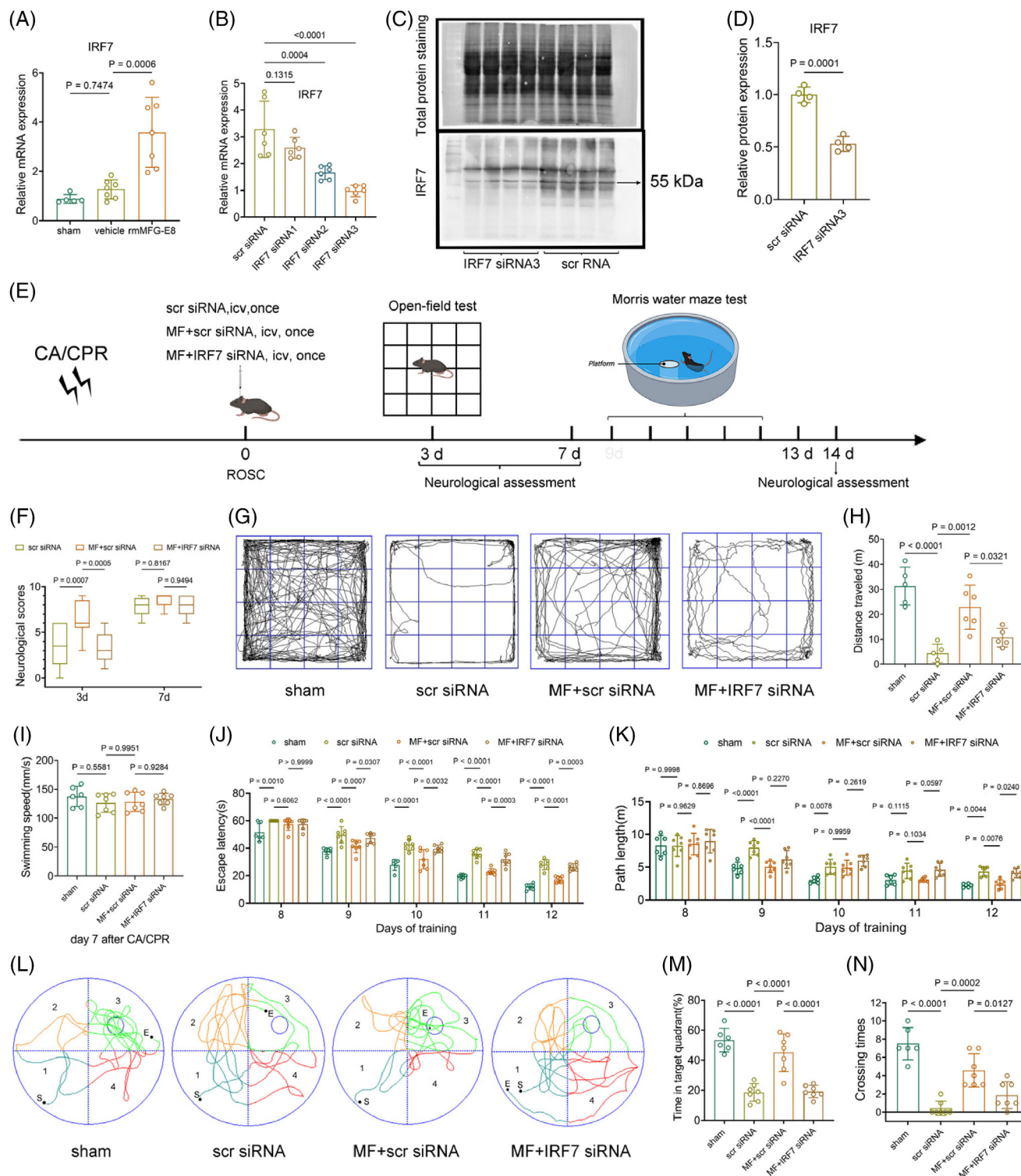
FIGURE 6 Effects of interferon regulatory factor 7 (IRF7) silence and recombinant mouse MFG-E8 (rmMFG-E8) administration on neurological function after cardiac arrest and cardiopulmonary resuscitation (CA/CPR). A. qPCR analysis of IRF7 expression of the sham group and the experimental groups on the 3rd day after CA/CPR. B. qPCR analysis of screening effective IRF7 siRNA. C, D. The Western Blot analysis of effective IRF7 siRNA. E. Experimental procedures of the next part. F. Neurological function scores in the different groups on the 3rd and 7th day after return of spontaneous circulation (ROSC). G. Representative tracks of mice in the different groups during the open field test. H. The total traveled distance of mice in the open field test. I. Average swimming speed in the Morris water maze test on the 7th day after surgery or ROSC. J. The escape latency of mice in different groups to find the platform in Morris water maze test. K. The swimming path length of mice during spatial exploration experiment. L. Representative swimming tracks of mice during the probe trial, S, start; E, end. M, N. The percentage of time in the target quadrant and the crossing times during the probe trial. Scr siRNA: Scramble siRNA, MF + scr siRNA: rmMFG-E8 + scramble siRNA, MF + IRF7 siRNA: RmMFG-E8 + IRF7 siRNA. i.c.v., intracerebroventricular injection.
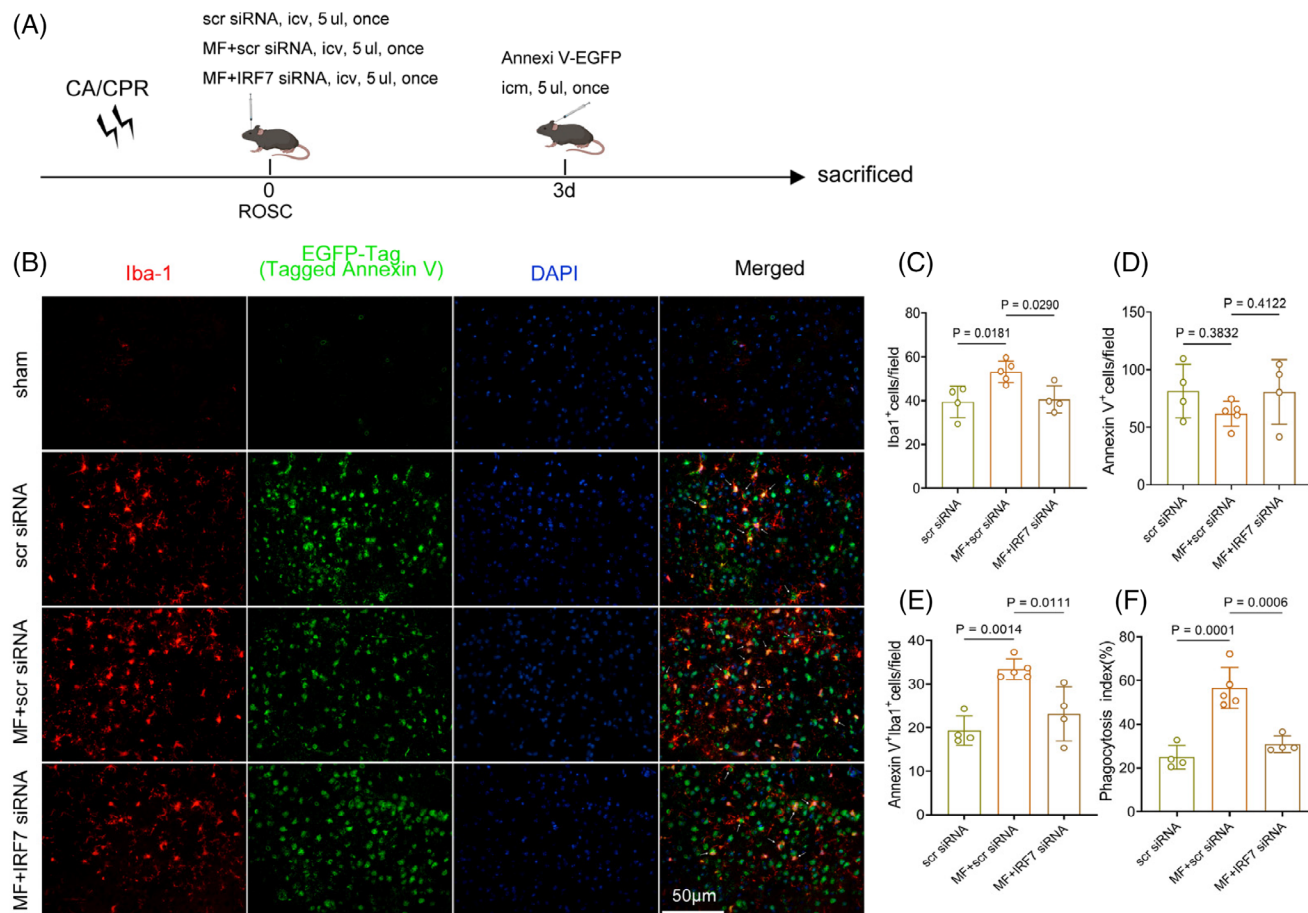
FIGURE 7 Effects of interferon regulatory factor 7 (IRF7) silence and recombinant mouse MFG-E8 (rmMFG-E8) administration on efferocytosis after cardiac arrest and cardiopulmonary resuscitation (CA/CPR). A. Experimental procedures of this part. B. Double immunofluorescence labeling for EGFP-Tagged Annexin V (green), Iba1 (red), and 4,6-diamidino-2-phenylindole (DAPI) (blue) on the 3rd day after CA/CPR. The arrows indicated the process of efferocytosis: Touching, enwrapping, and engulfing. Scale bar: 50 μm. C. The number of microglia (Iba1$^+$) in each group after CA/CPR. D. The number of cells with phosphatidylserine (PS) eversion (AnnexinV$^+$) on the 3rd day of the three groups. E. The number of PS eversion cells involved in efferocytosis (AnnexinV$^+$Iba1$^+$) on the 3rd day after CA/CPR. F. The phagocytosis index represented by AnnexinV$^+$Iba1$^+$/AnnexinV$^+$ × 100% in each group. Scr siRNA: Scramble siRNA, MF + scr siRNA: rmMFG-E8 + scramble siRNA, MF + IRF7 siRNA: rmMFG-E8 + IRF7 siRNA. i.c.m., intra-cisterna magna injection; i.c.v., intracerebroventricular injection; ROSC, return of spontaneous circulation.

significantly shortened swimming distances to find the hidden platform on the 9th day and 12th day (all p <0.01 vs. scrambled siRNA) (Figure 6K). However, the swimming distances of mice were partly lengthened on the 12th day in the rmMFG-E8 + IRF7 siRNA group (p <0.05 vs. rmMFG-E8 + scrambled siRNA) (Figure 6K). We performed the probe test to assess short-term memory in different groups on the 13th day after CA/CPR (Figure 6L). The results showed that the frequency of scrambled siRNA group crossing the platform was less than the sham group, and the rmMFG-E8 + scramble siRNA group reversed this trend, while the crossing times in rmMFG-E8 + IRF7 siRNA group were less than the rmMFG-E8 + scramble siRNA group (Figure 6N). Moreover, rmMFG-E8 + scramble siRNA-treated mice spent significantly more time searching the platform quadrant (Q3) compared with scramble siRNA-treated mice, while the rmMFG-E8 + IRF7

siRNA-treated mice spent less time searching the platform quadrant compared with rmMFG-E8 + scramble siRNA-treated mice (Figure 6M). These results suggest that IRF7 is involved in mediating the neuroprotection of rmMFG-E8 after CA/CPR.

3.7 | MFG-E8/IRF7 signaling axis may be involved in the microglial efferocytosis and polarization after CA/CPR

We performed immunofluorescence analysis to determine the number of injured cells and efferocytosis of microglia in each group on the 3rd day after CA/CPR (Figure 7A,B). The sham-operated group was excluded from the statistical analysis due to the very low number of PS eversion cells. The criteria for efferocytosis inclusion remained the same as before. The study results

FIGURE 8 Effects of interferon regulatory factor 7 (IRF7) silence and recombinant mouse MFG-E8 (rmMFG-E8) administration on microglia polarization and inflammation response after cardiac arrest and cardiopulmonary resuscitation (CA/CPR). A. Experimental procedures of this part. B, C. Immunofluorescence labeling on the 3rd day after CA/CPR with Iba1 (red) labeling microglia, iNOS (green) as a marker of proinflammatory phenotype of microglia, and Arg1 (green) representing anti-inflammatory phenotype of microglia. Scale bar: 50 μm. D, E. Quantification of the percentage of iNOS and Iba1 double-positive cells as well as Arg1 and Iba1 double-positive cells. F–J. qPCR analysis of proinflammatory and anti-inflammatory markers expression following IRF7 silence and rmMFG-E8 administration in different groups. Scr siRNA: scramble siRNA, MF + scr siRNA: rmMFG-E8 + scramble siRNA, MF + IRF7 siRNA: rmMFG-E8 + IRF7 siRNA. DAPI, 4,6-diamidino-2-phenylindole; i.c.v., intracerebroventricular injection; ROSC, return of spontaneous circulation.
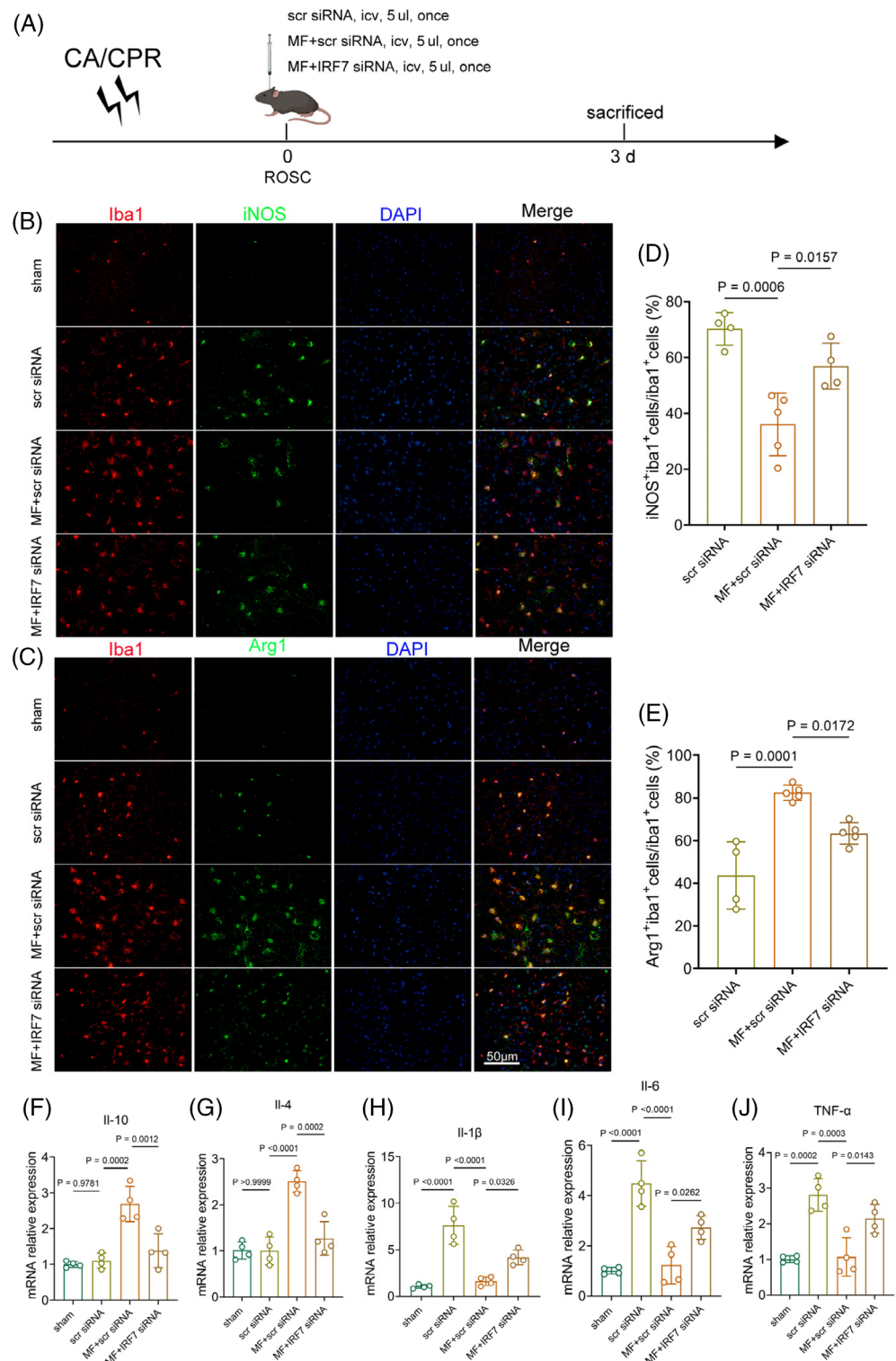
indicated that the number of PS eversion cells increased in the rmMFG-E8 + IRF7 siRNA group compared with the rmMFG-E8 + scrambled siRNA group, but the difference between the two groups was not statistically significant (Figure 7D). Compared with the rmMFG-E8 + scrambled siRNA group, the number of phagocytosed PS eversion cells by microglia and the phagocytosis index

were significantly lower in the rmMFG-E8 + IRF7 siRNA group on the 3rd day after CA/CPR (Figure 7E,F). Furthermore, the group treated with rmMFG-E8 + IRF7 siRNA exhibited a decrease in the number of microglia in comparison with the rmMFG-E8 + scrambled siRNA group (Figure 7C), which might be related to the lower phagocytosis index [31, 46].

Microglial polarization was analyzed by immunofluorescence in each group on the 3rd day after CA/CPR (Figure 8A). The results showed that the expression of the proinflammatory molecule iNOS was decreased in the rmMFG-E8 + scrambled siRNA group compared with the scrambled siRNA group, but increased in the rmMFG-E8 + IRF7 siRNA group compared with the rmMFG-E8 + scrambled siRNA group (Figure 8B,D). On the 3rd day after CA/CPR, the expression of the anti-inflammatory molecule Arg1 in microglia was increased after administration of rmMFG-E8 + scrambled siRNA compared with scrambled siRNA administration, whereas Arg1 expression in microglia was decreased after administration of rmMFG-E8 + IRF7 siRNA (Figure 8C,E). The qPCR analysis further demonstrated that the expression of anti-inflammatory markers, including Il-10 and Il-4, were significantly down-regulated (Figure 8F,G), while the expression of proinflammatory markers, such as Il-1β, Il-6, and TNF-α, were obviously elevated in the rmMFG-E8 + IRF7 siRNA group compared with rmMFG-E8 + scrambled siRNA group (Figure 8H–J). The above data indicate that the absence of IRF7 inhibits the neuroprotective effects of rmMFG-E8 against post-CA/CPR brain injury by impairing the efferocytosis and the microglial polarization towards the anti-inflammatory phenotype and aggravating the inflammatory response.

4 | DISCUSSION

This study investigated the neuroprotective effects of rmMFG-E8 and the potential molecular mechanisms after experimental CA/CPR in mice. We demonstrated that rmMFG-E8 administration enhanced microglial efferocytosis of apoptotic cells, improved 7-day survival rate and neurological outcome, and decreased histological damage. Additionally, rmMFG-E8 facilitated the transformation of microglia to an anti-inflammatory phenotype, possibly depending on the up-regulation of IRF7. These findings provide evidence that rmMFG-E8 protects against brain injury from CA/CPR by potentiating microglial efferocytosis.

Evidence has accumulated that recombinant MFG-E8 plays a neuroprotective role by inhibiting microglia-involved inflammation and reducing neuronal apoptosis in multiple central nervous system diseases [18–20]. Nakaya et al. [47] demonstrated that MFG-E8-dependent engulfment by cardiac myofibroblasts has a protective effect on the heart after myocardial infarction. Furthermore, myofibroblasts acquired anti-inflammatory properties after MFG-E8-mediated engulfment of apoptotic cells. In the brain, MFG-E8 treatment prompted the shift of microglia to an anti-inflammatory phenotype in both in vivo and in vitro models [20, 21]. In our study, we provided evidence that rmMFG-E8 administration significantly improved neurological outcomes and reduced histological injury, supporting MFG-E8 as a

promising strategy to combat post-CA/CPR brain injury, consistent with previous research [18–20]. As a step forward, we revealed that MFG-E8 administration enhanced microglia-mediated efferocytosis to engulf more PS-exposed dying cells and drove microglia to an anti-inflammatory phenotype, which may be mediated by up-regulation of IRF7. Collectively, it is suggested that MFG-E8 administration may improve neurological function by enhancing efferocytosis in the early period after CA/CPR, clearing the dying cells promptly, avoiding secondary necrosis, and attenuating inflammatory responses.

It should be noted that increased MFG-E8 appears to have a detrimental effect on aged mice and humans. A genetic deficiency in MFG-E8 attenuated age-related cerebrovascular function decline and age-related neuromuscular junction degeneration [48, 49]. We speculate that the main reason for this unfavorable effect of MFG-E8 is that the amount of MFG-E8 increases with age [49], and that more MFG-E8 enhances engulfment of synapses by astrocytes and microglia, especially in Alzheimer's disease [50]. That reminds us that the balance of beneficial and harmful effects of taking MFG-E8 varies in different disease models and at different stages of the disease. At the early stage of the acute injury models, exogenous administration of MFG-E8 can remove massive dying cells, thus alleviating the inflammation caused by the accumulation of dying cells due to the insufficiency of MFG-E8. However, in the chronic disease models or aged mice and humans, exogenous supplementation of MFG-E8 will have a detrimental effect due to the overexpression of MFG-E8. In the current study, we found that rmMFGE8 treatment significantly increased the number of microglia and thereby enhanced efferocytosis of apoptotic cells within 7 days, whereas the number of microglia decreased on the 14th day, suggesting that the rmMFGE8 intervention only works in the acute phase, making it a promising agent to combat post-CA/CPR brain injury.

The underlying mechanism of microglia shifting to an anti-inflammatory phenotype following rmMFG-E8 administration after CA/CPR has not been well elucidated. Our findings showed that rmMFG-E8 treatment induced up-regulation of IRF7, while gene knockdown of IRF7 largely reversed the neuroprotection of rmMFG-E8, indicating that IRF7 may be responsible for the microglial anti-inflammatory phenotype polarization mediated by rmMFG-E8. IRF7 has been reported to inhibit monocrotaline-induced NF-kB activation in pulmonary hypertension rats, significantly reducing levels of proinflammatory cytokines such as TNF-α and IL-6 [51]. Cohen et al. [44] also demonstrated that IRF7 plays a critical role in the M1 to M2 conversion of myeloid cells by negatively regulating the expression of inflammatory pathway genes such as Il-1β, TNF-α, Cxcl1, and Cxcl2, and up-regulating the expression of anti-inflammatory genes such as Il10. Moreover, a recent study has shown

that the IRF7 up-regulation also has neuroprotective effects in mice with postoperative neurocognitive impairment [45]. Our findings were in line with the above experimental results. However, IRF7 plays different roles in different disease models or cell types, which may result from the activation of multiple signaling pathways. The regulatory mechanisms of IRF7 and the signaling pathways of the IRF system deserve further investigation and may become important targets for treating inflammation-related diseases. In our experiment, we only used rmMFG-E8 and IRF7 siRNA, which may not be sufficient in confirming their causal relationship. Therefore, data from conditional gene knock-out mice (mfg-$e8^{-/-}$ and $IRF7^{-/-}$) and gene overexpression mice that specifically target the microglial MFG-E8 and IRF7 may be more convincing. In addition, we only examined the effects of the MFG-E8/IRF7 pathway on microglial polarization, and other MFG-E8 signaling pathways that affect microglial polarization should be further investigated.

5 | CONCLUSION

In conclusion, we characterize the neuroprotection of rmMFG-E8 in post-CA/CPR brain injury via reducing histological injury and improving neurological function. These protective effects of rmMFG-E8 are attributed to promoting the clearance of dying cells and facilitating the shift of microglia towards a neuroprotective phenotype, which may be related to the up-regulation of IRF7. Our work provides novel insights into the therapeutic potential of rmMFG-E8 to be a multipotent and promising agent in treating post-CA/CPR brain injury.

AUTHOR CONTRIBUTIONS

Kunxue Zhang, Yuzhen Zhang, Zhentong Li, Jiancong Chen, and Yuan Chang established the mouse model of CA/CPR. Kunxue Zhang, Yuzhen Zhang, Zhentong Li, and Yongchuan Li performed immunofluorescence experiments of brain tissue sections. Jiancong Chen, Yuan Chang, Shuxin Zeng, and Sifan Pan performed behavioral experiments. Kunxue Zhang, Yuzhen Zhang, and Zhentong Li contributed data analysis. Kaibin Huang, Suyue Pan, Kunxue Zhang, Yuzhen Zhang, and Zhentong Li verified the underlying data. Kunxue Zhang, Yuzhen Zhang, Zhentong Li, and Yuan Chang wrote the manuscript. Kaibin Huang and Suyue Pan revised the manuscript. All authors read and approved the final version of the manuscript.

CONFLICT OF INTEREST STATEMENT

The authors declare that they have no competing interests.

DATA AVAILABILITY STATEMENT

The data that supports the findings of this study are available in the supplementary material of this article.

ETHICS STATEMENT

All animal experiments in this study were approved by Animal Care and Use Committee of Nanfang Hospital, Southern Medical University (Guangzhou, China) (Approval No. IACUC-LAC-20220708-006).

ORCID

Kunxue Zhang https://orcid.org/0009-0004-2398-1750
Jiancong Chen https://orcid.org/0000-0001-8796-5208
Suyue Pan https://orcid.org/0000-0003-2744-1984
Kaibin Huang https://orcid.org/0000-0002-3360-7031

REFERENCES

1. Tsao CW, Aday AW, Almarzooq ZI, Anderson CAM, Arora P, Avery CL, et al. Heart disease and stroke statistics-2023 update: a report from the American Heart Association. Circulation. 2023; 147(8):e459. https://doi.org/10.1161/CIR.0000000000001123

2. Zheng J, Lv C, Zheng W, Zhang G, Tan H, Ma Y, et al. Incidence, process of care, and outcomes of out-of-hospital cardiac arrest in China: a prospective study of the BASIC-OHCA registry. Lancet Public Health. 2023;8(12):e923–32. https://doi.org/10.1016/S2468-2667(23)00173-1

3. Zhang Y, Li Z, Zhang K, Chang Y, Chen J, Al-Nusaif M, et al. Inflammatory responses involved in post-cardiac arrest brain injury: mechanisms, regulation, and therapeutic potential. Expl Neurosci. 2023;2(2):82–97. https://doi.org/10.37349/en.2023.00014

4. Perkins GD, Callaway CW, Haywood K, Neumar RW, Lilja G, Rowland MJ, et al. Brain injury after cardiac arrest. Lancet. 2021; 398(10307):1269–78. https://doi.org/10.1016/S0140-6736(21)00953-3

5. Newton K, Dixit VM, Kayagaki N. Dying cells fan the flames of inflammation. Science. 2021;374(6571):1076–80. https://doi.org/10.1126/science.abi5934

6. deCathelineau AM, Henson PM. The final step in programmed cell death: phagocytes carry apoptotic cells to the grave. Essays Biochem. 2003;39:105–17.

7. Li Q, Barres BA. Microglia and macrophages in brain homeostasis and disease. Nat Rev Immunol. 2018;18(4):225–42. https://doi.org/10.1038/nri.2017.125

8. Monks J, Rosner D, Geske FJ, Lehman L, Hanson L, Neville MC, et al. Epithelial cells as phagocytes: apoptotic epithelial cells are engulfed by mammary alveolar epithelial cells and repress inflammatory mediator release. Cell Death Differ. 2005; 12(2):107–14.

9. Arandjelovic S, Ravichandran KS. Phagocytosis of apoptotic cells in homeostasis. Nat Immunol. 2015;16(9):907–17. https://doi.org/10.1038/ni.3253

10. Sachet M, Liang YY, Oehler R. The immune response to secondary necrotic cells. Apoptosis. 2017;22(10):1189–204. https://doi.org/10.1007/s10495-017-1413-z

11. Boada-Romero E, Martinez J, Heckmann BL, Green DR. The clearance of dead cells by efferocytosis. Nat Rev Mol Cell Biol. 2020;21(7):398–414. https://doi.org/10.1038/s41580-020-0232-1

12. Szondy Z, Garabuczi E, Joós G, Tsay GJ, Sarang Z. Impaired clearance of apoptotic cells in chronic inflammatory diseases: therapeutic implications. Front Immunol. 2014;5:354. https://doi.org/10.3389/fimmu.2014.00354

13. Stubbs JD, Lekutis C, Singer KL, Bui A, Yuzuki D, Srinivasan U, et al. cDNA cloning of a mouse mammary epithelial cell surface protein reveals the existence of epidermal growth factor-like domains linked to factor VIII-like sequences. Proc Natl Acad Sci U S A. 1990;87(21):8417–21.

14. Hanayama R, Tanaka M, Miwa K, Shinohara A, Iwamatsu A, Nagata S. Identification of a factor that links apoptotic cells to phagocytes. Nature. 2002;417(6885):182–7.

15. Akakura S, Singh S, Spataro M, Akakura R, Kim JI, Albert ML, et al. The opsonin MFG-E8 is a ligand for the alphavbeta5 integrin and triggers DOCK180-dependent Rac1 activation for the phagocytosis of apoptotic cells. Exp Cell Res. 2004;292(2):403–16.

16. Aziz M, Jacob A, Matsuda A, Wang P. Review: milk fat globule-EGF factor 8 expression, function and plausible signal transduction in resolving inflammation. Apoptosis. 2011;16(11):1077–86. https://doi.org/10.1007/s10495-011-0630-0

17. Miksa M, Wu R, Dong W, Das P, Yang D, Wang P. Dendritic cell-derived exosomes containing milk fat globule epidermal growth factor-factor VIII attenuate proinflammatory responses in sepsis. Shock. 2006;25(6):586–93.

18. Gao Y-Y, Zhang Z-H, Zhuang Z, Lu Y, Wu LY, Ye ZN, et al. Recombinant milk fat globule-EGF factor-8 reduces apoptosis via integrin β3/FAK/PI3K/AKT signaling pathway in rats after traumatic brain injury. Cell Death Dis. 2018;9(9):845. https://doi.org/10.1038/s41419-018-0939-5

19. Cheyuo C, Jacob A, Wu R, Zhou M, Qi L, Dong W, et al. Recombinant human MFG-E8 attenuates cerebral ischemic injury: its role in anti-inflammation and anti-apoptosis. Neuropharmacology. 2012;62(2):890–900. https://doi.org/10.1016/j.neuropharm.2011.09.018

20. Gao Y-Y, Tao T, Wu D, Zhuang Z, Lu Y, Wu LY, et al. MFG-E8 attenuates inflammation in subarachnoid hemorrhage by driving microglial M2 polarization. Exp Neurol. 2021;336:113532. https://doi.org/10.1016/j.expneurol.2020.113532

21. Shi X, Cai X, Di W, Li J, Xu X, Zhang A, et al. MFG-E8 selectively inhibited Aβ-induced microglial M1 polarization via NF-κB and PI3K-Akt pathways. Mol Neurobiol. 2017;54(10):7777–88. https://doi.org/10.1007/s12035-016-0255-y

22. Wang W, Li R, Miao W, Evans C, Lu L, Lyu J, et al. Development and evaluation of a novel mouse model of Asphyxial cardiac arrest revealed severely impaired lymphopoiesis after resuscitation. J Am Heart Assoc. 2021;10(11):e019142. https://doi.org/10.1161/JAHA.120.019142

23. Combs DJ, D'Alecy LG. Motor performance in rats exposed to severe forebrain ischemia: effect of fasting and 1,3-butanediol. Stroke. 1987;18(2):503–11.

24. Vorhees CV, Williams MT. Morris water maze: procedures for assessing spatial and related forms of learning and memory. Nat Protoc. 2006;1(2):848–58.

25. Zhu J, Liu K, Huang K, Gu Y, Hu Y, Pan S, et al. Metformin improves neurologic outcome via AMP-activated protein kinase-mediated autophagy activation in a rat model of cardiac arrest and resuscitation. J Am Heart Assoc. 2018;7(12):3. https://doi.org/10.1161/JAHA.117.008389

26. Chang Y, Zhu J, Wang D, Li H, He Y, Liu K, et al. NLRP3 inflammasome-mediated microglial pyroptosis is critically involved in the development of post-cardiac arrest brain injury. J Neuroinflammation. 2020;17(1):219. https://doi.org/10.1186/s12974-020-01879-1

27. Plemel JR, Stratton JA, Michaels NJ, Rawji KS, Zhang E, Sinha S, et al. Microglia response following acute demyelination is heterogeneous and limits infiltrating macrophage dispersion. Sci Adv. 2020;6(3):eaay6324. https://doi.org/10.1126/sciadv.aay6324

28. Wang L, Li H, Tang Y, Yao P. Potential mechanisms and effects of efferocytosis in atherosclerosis. Front Endocrinol. 2020;11:585285. https://doi.org/10.3389/fendo.2020.585285

29. Wang M, Fu Z, Wu J, Zhang J, Jiang L, Khazan B, et al. MFG-E8 activates proliferation of vascular smooth muscle cells via integrin signaling. Aging Cell. 2012;11(3):500–8. https://doi.org/10.1111/j.1474-9726.2012.00813.x

30. Li H, Xu W, Ma Y, Zhou S, Xiao R. Milk fat globule membrane protein promotes C2C12 cell proliferation through the PI3K/Akt signaling pathway. Int J Biol Macromol. 2018;114:1305–14. https://doi.org/10.1016/j.ijbiomac.2018.04.026

31. Ngai D, Schilperoort M, Tabas I. Efferocytosis-induced lactate enables the proliferation of pro-resolving macrophages to mediate tissue repair. Nat Metab. 2023;5(12):2206–19. https://doi.org/10.1038/s42255-023-00921-9

32. Yurdagul A, Subramanian M, Wang X, Crown SB, Ilkayeva OR, Darville L, et al. Macrophage metabolism of apoptotic cell-derived arginine promotes continual efferocytosis and resolution of injury. Cell Metab. 2020;31(3):518–533.e10. https://doi.org/10.1016/j.cmet.2020.01.001

33. Reis C, Akyol O, Araujo C, Huang L, Enkhjargal B, Malaguit J, et al. Pathophysiology and the monitoring methods for cardiac arrest associated brain injury. Int J Mol Sci. 2017;18(1):3–5. https://doi.org/10.3390/ijms18010129

34. Cai W, Dai X, Chen J, Zhao J, Xu M, Zhang L, et al. STAT6/Arg1 promotes microglia/macrophage efferocytosis and inflammation resolution in stroke mice. JCI Insight. 2019;4(20):6–7. https://doi.org/10.1172/jci.insight.131355

35. Hazelton JL, Balan I, Elmer GI, Kristian T, Rosenthal RE, Krause G, et al. Hyperoxic reperfusion after global cerebral ischemia promotes inflammation and long-term hippocampal neuronal death. J Neurotrauma. 2010;27(4):753–62. https://doi.org/10.1089/neu.2009.1186

36. Tuo Q-Z, Liuyang Z-Y, Lei P, Yan X, Shentu YP, Liang JW, et al. Zinc induces CDK5 activation and neuronal death through CDK5-Tyr15 phosphorylation in ischemic stroke. Cell Death Dis. 2018;9(9):870. https://doi.org/10.1038/s41419-018-0929-7

37. Park J-S, Manzanero S, Chang J-W, Choi Y, Baik SH, Cheng YL, et al. Calsenilin contributes to neuronal cell death in ischemic stroke. Brain Pathol. 2013;23(4):402–12. https://doi.org/10.1111/bpa.12013

38. Liddelow S, Barres B. SnapShot: astrocytes in health and disease. Cell. 2015;162(5):1170–1170.e1. https://doi.org/10.1016/j.cell.2015.08.029

39. Brennan FH, Li Y, Wang C, Ma A, Guo Q, Li Y, et al. Microglia coordinate cellular interactions during spinal cord repair in mice. Nat Commun. 2022;13(1):4096. https://doi.org/10.1038/s41467-022-31797-0

40. Voet S, Srinivasan S, Lamkanfi M, van Loo G. Inflammasomes in neuroinflammatory and neurodegenerative diseases. EMBO Mol Med. 2019;11(6):5–7. https://doi.org/10.15252/emmm.201810248

41. Chen J, Chang Y, Zhu J, Peng Y, Li Z, Zhang K, et al. Flufenamic acid improves survival and neurologic outcome after successful cardiopulmonary resuscitation in mice. J Neuroinflammation. 2022;19(1):214. https://doi.org/10.1186/s12974-022-02571-2

42. Zhang S, Weinberg S, DeBerge M, Gainullina A, Schipma M, Kinchen JM, et al. Efferocytosis fuels requirements of fatty acid oxidation and the electron transport chain to polarize macrophages for tissue repair. Cell Metab. 2019;29(2):443–456.e5. https://doi.org/10.1016/j.cmet.2018.12.004

43. Honda K, Yanai H, Negishi H, Asagiri M, Sato M, Mizutani T, et al. IRF-7 is the master regulator of type-I interferon-dependent immune responses. Nature. 2005;434(7034):772–7.

44. Cohen M, Matcovitch O, David E, Barnett-Itzhaki Z, Keren-Shaul H, Blecher-Gonen R, et al. Chronic exposure to TGFβ1 regulates myeloid cell inflammatory response in an IRF7-dependent manner. EMBO J. 2014;33(24):2906–21. https://doi.org/10.15252/embj.201489293

45. Zhang X-J, Wang Z, Chen J-W, Yuan SY, Zhao L, Zhong JY, et al. The neuroprotective effect of near infrared light therapy in aged mice with postoperative neurocognitive disorder by upregulating IRF7. J Affect Disord. 2024;349:297–309. https://doi.org/10.1016/j.jad.2024.01.074

46. Gerlach BD, Ampomah PB, Yurdagul A, Liu C, Lauring MC, Wang X, et al. Efferocytosis induces macrophage proliferation to help resolve tissue injury. Cell Metab. 2021;33(12):2445–2463.e8. https://doi.org/10.1016/j.cmet.2021.10.015

47. Nakaya M, Watari K, Tajima M, Nakaya T, Matsuda S, Ohara H, et al. Cardiac myofibroblast engulfment of dead cells facilitates recovery after myocardial infarction. J Clin Invest. 2017;127(1):383–401. https://doi.org/10.1172/JCI83822

48. Degenhardt K, Wagner J, Skodras A, Candlish M, Koppelmann AJ, Wild K, et al. Medin aggregation causes cerebrovascular dysfunction in aging wild-type mice. Proc Natl Acad Sci U S A. 2020;117(38):23925–31. https://doi.org/10.1073/pnas.2011133117

49. Ikemoto-Uezumi M, Zhou H, Kurosawa T, Yoshimoto Y, Toyoda M, Kanazawa N, et al. Increased MFG-E8 at neuromuscular junctions is an exacerbating factor for sarcopenia-associated denervation. Aging Cell. 2022;21(1):e13536. https://doi.org/10.1111/acel.13536

50. Tzioras M, Daniels MJD, Davies C, Baxter P, King D, McKay S, et al. Human astrocytes and microglia show augmented ingestion of synapses in Alzheimer's disease via MFG-E8. Cell Rep Med. 2023;4(9):101175. https://doi.org/10.1016/j.xcrm.2023.101175

51. Deng Y, Guo S-L, Li J-Q, Xie SS, Zhou YC, Wei B, et al. Interferon regulatory factor 7 inhibits rat vascular smooth muscle cell proliferation and inflammation in monocrotaline-induced pulmonary hypertension. Life Sci. 2021;264:118709. https://doi.org/10.1016/j.lfs.2020.118709

SUPPORTING INFORMATION

Additional supporting information can be found online in the Supporting Information section at the end of this article.